

Biological Effects of Ceramic-coating on Titanium

Sung-Hwa Sohn¹, Jae Bum Lee², Ki-Nam Kim¹,
Hye Won Kim¹, In Kyoung Kim¹, Seung Ho Lee¹,
Sang-Hui Seo¹, Yu-Ri Kim¹, Seung Min Lee¹,
Sang-Wan Shin², Jae-Jun Ryu²
& Meyoung-Kon Kim¹

¹Department of Biochemistry & Molecular Biology,

²Department of Dentistry, College of Medicine, Korea University,
Seoul 136-705, Korea

Correspondence and requests for materials should be addressed
to M-K. Kim (jerrykim@korea.ac.kr)

Accepted 18 May 2006

Abstract

Several features of the implant surface, such as roughness, topography, and composition play a relevant role in implant integration with bone. This study was conducted in order to determine the effects of ceramic-coatings on Ti surfaces on the biological responses of a human osteoblast-like cell line (MG63). MG63 cells were cultured on Zr (Zirconium-coated surface), Nb (Niobium-coated surface), and control (Uncoated Titanium) Ti. The morphology of these cells was assessed by SEM. The cDNAs prepared from the total RNAs of the MG63 were hybridized into a human cDNA microarray (1,152 elements). The appearances of the surfaces observed by SEM were different on each of the three dental substrate types. MG63 cells cultured on Zr, Nb and control exhibited cell-matrix interactions. In the expression of several genes were up-, and down-regulated on the different surfaces. The attachment and expression of key osteogenic regulatory genes were enhanced by the surface morphology of the dental materials used.

Keywords: Titanium, Zr coating, Nb coating, Gene expression profiling, cDNA microarray

Titanium (Ti) and its alloys have been widely used for orthopedic implants that interact with bone cells *in vitro* and *in vivo*¹. For decades, oral, maxillofacial, and orthopedic surgeons have placed dental implants, screws and plates, and prostheses to substitute lost teeth, to fix bone fragments, and to replace joints, respectively. Also, many surgical instruments, such

as drills and saws, are made with Ti alloys. However, the exact effect of Ti on osteoblasts is still unknown²⁻⁴. Successful application of such materials for bone regeneration often involved mixing with autogenous bone, a source of osteoblastic cells and precursors².

Surface topography may affect the formation of a fibrous capsule around implants, inflammatory response at tissue-implant interface, fibroblast attachment, angiogenesis, epithelial down-growth around percutaneous devices, and many cellular processes such as cellular differentiation, DNA/RNA transcription, cell metabolism, protein production, and phenotypic expression^{1,3,5-7}. Diverse implant surface may contribute to the regulation of osteoblast differentiation by influencing the level of gene expression of key osteogenic factors^{7,8}. Morphometric analyses had shown differences in bone-implant contact percentages with the varying of surface characteristics, as well as a sensitivity of cells to surface topography^{9,10}. Gene expression in response to the placement of implants with different surface topographies¹¹⁻¹⁴. Bio-material composition and surface topography regulate cell attachment, focal contact formation and cytoskeletal organization with long-term effects on osteoblastic cell maturation, and subsequent mineralization¹⁵.

We hypothesized that ceramic-coatings on Ti surface conditions would be associated with differential bone-matrix gene expression and interfacial strengths, which may lead to the development of more advanced therapeutic prosthetic interventions associated with dental implant therapy and tissue-engineering biological applications.

Scanning electron microscopic (SEM) examinations revealed morphologic differences in the MG63 cells which adhered to different ceramic-coating Ti surfaces. Cell growth was observed on control, Zr, and Nb. Fig. 1 presents the morphology and size of cell on the Ti surface. Control surface showed cell-cell interaction. Zr sample was observed that the shapes of cells having many pseudopodia are short and thin, and showed cell-matrix. Nb sample was showed cell-matrix interaction. These results showed that demonstrating good attachment potential to Zr Ti. Figure 2 is scatter plot for comparing the expression profiles of different ceramic-coatings on Ti and control. Regeneration analysis of Z scores from two independent samples of different ceramic-coatings on Ti and control were performed and Z scores of indi-

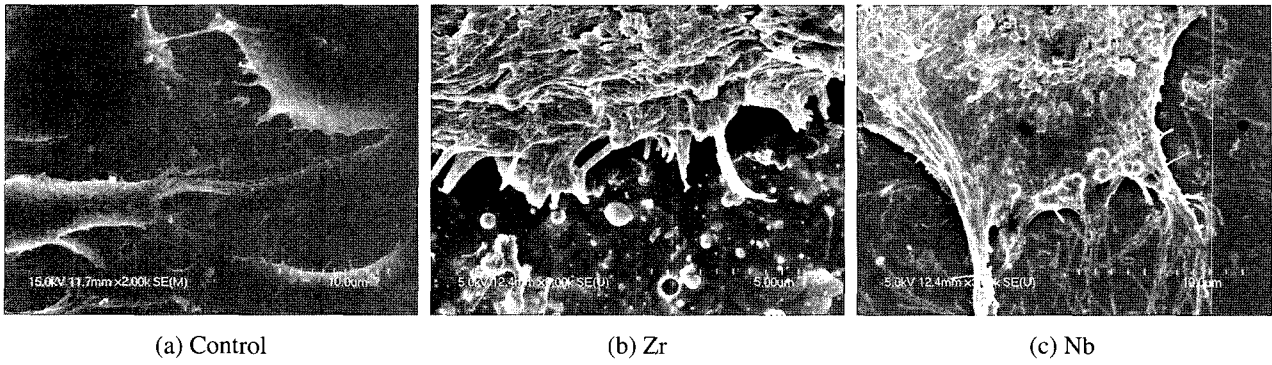


Fig. 1. SEM images of MG63 cells attached on Ti surfaces with different ceramic coating (3 day culture, $\times 3,000$): (a) the control (Non-ceramic coating on Ti surface) surface showing cell- cell interaction; (b) the Zr (Zirconium coating on Ti surface) surface showing cell- matrix interaction; (c) the Nb (Niobium coating on anodized surface) surface showing cell-matrix interaction.

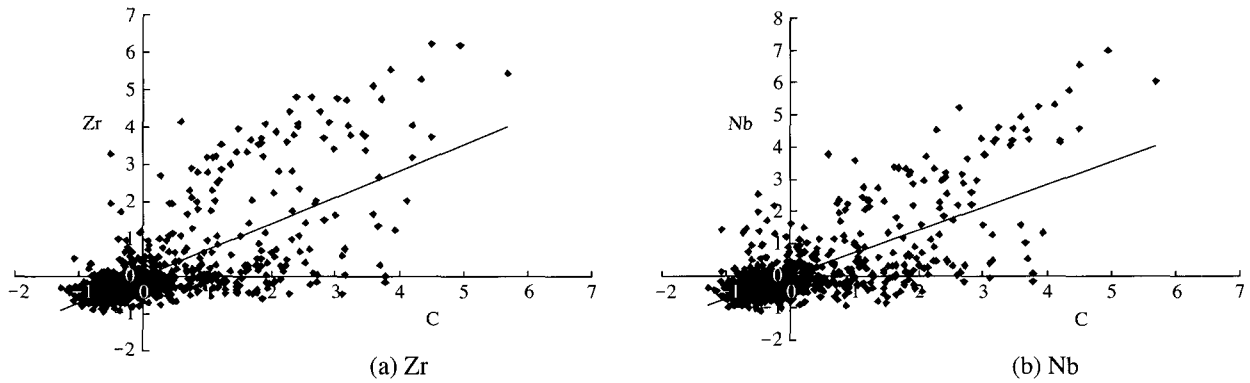


Fig. 2. Scatter plots for comparison of expression profile between control and different ceramic coating on Ti surface. Expression profiles of non-ceramic coating Smooth (control) versus different ceramic coating on Ti surface on MG63 cells. (a) Zr (Zirconium coating on Ti surface) on MG63 cells versus control; (b) Nb (Niobium coating on Ti surface) on MG63 cells versus control are shown as bivariate scatter plots of 1,152 genes from the microarray. The values are corrected intensities relative to control, representing levels of expression for the DNA elements of the microarrays.

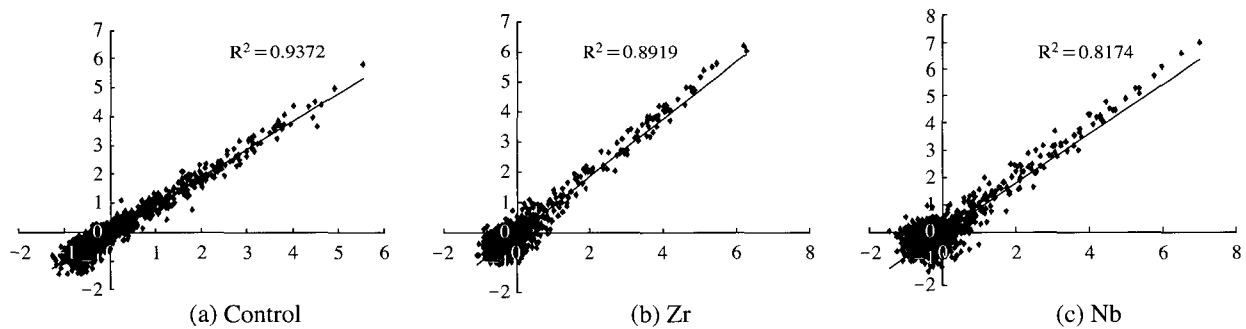


Fig. 3. Microarray reproducibility. Each microarray contains two identical grids. Regression analysis of Z scores from three samples of controls, Zr, and Nb coating on Ti surface treated MG63 cells were performed. Z scores of individual genes from each member of duplicates were plotted, and the relationship between three samples was calculated to obtain R^2 . Based on R^2 , microarray hybridization patterns were found to be highly consistent between the samples. A perfect relationship between samples would be a slope of 1.


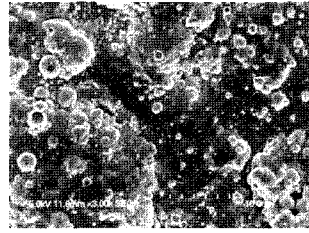

vidual genes were plotted. To assess the reliability of microarray technique used, we calculated microarray reproducibility between duplicates (Fig. 3). The duplicate genetic elements for each microarray resulted in two separate Z normalizations and an average Z score for each gene. The scatter plot for Z scores in the cells grown on control, Zr, and Nb Ti samples showed R2 across duplicates of 0.96, 0.89, and 0.82, respectively (Fig. 3). A perfect relationship between duplicates would be a slope of 1. The average coefficient of variation for duplicate Z scores within each microarray was below 20% approximately, indicating a high reliability of our microarray data. Table 2 shows the expression of various genes in different Ti surfaces compared with the control group.

Discussion

The frequently observed unwanted biological effects of different metals require in vitro and in vivo biological tests of any medical or dental device before its definite use in humans. Biological testing of medical and dental devices is necessary in order to evaluate the biological behaviour of biomaterials. The cell-matrix interaction morphology could be observed on the Zr surfaces, the surface morphology of which were observed by SEM to be rougher than those of other Ti samples (Table 1, fig. 1). Osteoblastic cells began to secrete several extracellular matrix (ECM) proteins. They will also attach on the implant surface and are necessary for adhesion due to their specific binding to cell surface receptors. The formation of cell attachment to the alloys seems to be slower than on pure Ti. A reasonable explanation for this observation is that the formation of cell-implant contacts may be hampered on rough surfaces^{16,17} while Carinci *et al.*¹⁸ and Lossdorfer *et al.*¹⁹ demonstrated that surface roughness affects proliferation, differentiation, local factor production. And alkaline phosphatase, osteocalcin, and Transforming Growth Factor beta were increased on the rougher surfaces. We also attempted to determine the effects of different Implant surfaces on the phenotype and gene expression of MG63 cells. In the experimental cultures, several genes were up-regulated or down-regulated. These genes were categorized depending on their functions, as follows (Table 2).

The FGFR (fibroblast growth factor receptor) family members include FGFR3 and FGFR12. The extracellular portion of the protein interacts with FGF, setting in motion a cascade of downstream signals, ultimately influencing mitogenesis and differentiation. This particular family member binds

Table 1. The surface morphology & characteristics.

Coating		Surface morphology
Control	Non-coating on Titanium	
Zr	Zirconium coating on Titanium	
Nb	Niobium coating on Titanium	

*Magnification 3000X, Ti surface morphology using a scanning electron microscopy (SEM).

acidic and basic FGF hormone and plays a role in bone development and maintenance. FGF was combined with BMP, FGF prevented the differentiating action of BMP. The FGF was loosely bound to the matrix. Also, FGF signaling inhibited expression of alkaline phosphatase (ALKP) and blocked mineralization in osteoblastic cells²⁰. In our study FGFR3 and FGFR12 were down-regulated in cultures grown on Zr and Nb. Integrins are heterodimeric integral membrane glycoproteins composed of an alpha chain and a beta chain that mediate cell-cell and cell-matrix adhesion. The protein encoded by this gene, when bound to the beta 1 chain, forms an integrin that is a receptor for VCAM1, cytotactin and osteopontin. Also, in our experiment, we noted the up-regulation of Integrin alpha 9 on Zr and Nb surfaces. Gap junctions were specialized structures on plasma membranes of contacting adherent cells. These structures were shown to consist of cell-to-cell channels. Proteins, called connexins, are designated by their molecular mass. Another system of nomenclature divides gap junction proteins into 2 categories, alpha and beta. Gap junction protein beta 2 is up-regulated in cultures grown on Nb.

Table 2. Up-and down-regulated Genes of ceramic-coatings on Ti surface.

Genes	Abb.	Regulation profile and Z-ratio	
		Zr	Nb
Signal transduction group			
calmodulin 3 (phosphorylase kinase, delta)	CALM3	3.22	-0.11
interleukin 2 receptor, alpha	CD25	3.20	-0.74
platelet-derived growth factor receptor, beta polypeptide	PDGFRB	3.03	1.30
EphB3	EPHB3	2.85	3.09
Bruton agammaglobulinemia tyrosine kinase	BTK	2.27	2.81
chemokine (C-C motif) receptor 5	CCR5	2.23	1.92
RYK receptor-like tyrosine kinase	RYK	2.17	1.54
adrenergic, beta-2-, receptor, surface	ADRB2	2.02	1.63
TCR adaptor molecule cbl-b	CBLB	-3.60	-2.48
anti-Mullerian hormone receptor, type II	AMHR2	-3.58	-3.25
EphA3	EPHA3	-3.43	-3.48
interleukin 12B	IL12B	-2.94	-2.56
G protein-coupled receptor 37 (endothelin receptor type B-like)	GPR37	-2.90	-3.45
CAMP responsive element binding protein 1	CREB1	-2.49	-2.36
interferon (alpha, beta and omega) receptor 1	IFNAR1	-2.46	-2.87
G protein-coupled receptor 9; CXCR3	GPR9	-2.12	-0.22
complement component 5 receptor 1 (C5a ligand)	C5R1	-2.11	-2.20
interleukin 9 receptor	IL9R	-2.09	-1.41
gap junction protein, beta 2, 26 kD (connexin 26)	GJB2	0.08	3.31
adaptor protein with pleckstrin homology and src homology 2 domains	APS	-0.32	2.85
thyroid stimulating hormone receptor	TSHR	1.61	2.79
regulator of G-protein signalling 1	RGS1	0.27	2.57
mitogen-activated protein kinase kinase kinase kinase 2	MAP4K2	-0.16	2.13
protein phosphatase 2, regulatory subunit B (B56), alpha isoform	PPP2R5A	0.35	2.12
budding uninhibited by benzimidazoles 1 (yeast homolog), beta	BUB1B	-0.83	-2.45
SHC (Src homology 2 domain-containing) transforming protein 1	SHC1	-1.93	-2.19
Apoptosis and anti-apoptosis related group			
TIA1 cytotoxic granule-associated RNA-binding protein-like 1	TIAL1	2.78	0.32
amyloid beta (A4) precursor protein	APP	2.62	2.28
caspase 1	CASP1	2.34	3.48
amyloid beta (A4) precursor protein (protease nexin-II)	APP	-5.01	-5.06
apoptosis-associated tyrosine kinase	AATK	-3.57	-3.53
neuronal thread protein AD7c-NTP	AD7CNTP	-2.83	-2.78
synuclein, alpha (non A4 component of amyloid precursor)	SNCA	-2.78	1.65
tumor necrosis factor receptor superfamily, member 1B	TNFRSF1B	-2.75	-1.81
death effector domain-containing protein	DEDD	-2.55	-2.72
tumor protein p53 (Li-Fraumeni syndrome)	TP53	-2.55	-2.42
annexin A5	ANX5	-2.03	-2.30
deoxyribonuclease II, lysosomal	DNASE2	-2.01	-1.82
nucleolar protein 3 (apoptosis repressor with CARD domain)	NOL3	0.46	2.93
Cell adhesion related group			
villin2	VIL2	2.49	1.75
integrin, alpha 9	ITGA9	2.30	2.11
selectin E (endothelial adhesion molecule 1)	SELE	-2.99	-3.18
claudin 3	CLDN3	-1.95	-2.06
Transcription group			
jun activation domain binding protein	JAB1	5.03	4.17
zinc finger protein ZNF49	ZNF49	3.28	3.43
protein phosphatase 1, regulatory subunit 10	PPP1R10	2.93	0.06
interferon regulatory factor 6	IRF6	2.46	1.18
suppressor of Ty (<i>S.cerevisiae</i>) 4 homolog 1	SUPT4H1	2.00	1.86
retinoblastoma-like 1 (p107)	RBL1	-5.23	-5.37
tailless homolog (<i>Drosophila</i>)	TLX	-4.11	-3.65
MAD (mothers against decapentaplegic, <i>Drosophila</i>) homolog 5	MADH5	-3.78	-3.91
MAX protein; helix-loop-helix zipper protein (max)	MAX	-3.73	-0.54
upstream transcription factor 2, c-fos interacting	USF2	-3.20	-2.55

Table 2. Continued.

Genes	Abb.	Regulation profile and Z-ratio	
		Zr	Nb
POU domain, class 2, associating factor 1	POU2AF1	-2.88	-3.05
transcription elongation factor S-II, hS-II-T1	TEFS2	-2.76	-3.00
core-binding factor, runt domain, alpha subunit 2; translocated to, 1	CBFA2T1	-2.16	-2.25
E2F transcription factor 3	E2F3	-0.72	2.22
CCAAT/enhancer binding protein (C/EBP), delta	CEBPD	-1.83	-2.21
Translation			
eukaryotic initiation factor 4A-I	EIF4AI	3.26	-3.18
ribosomal protein L7a	RPL7A	-3.39	-3.70
ribosomal protein S25	RPS25	-1.53	-2.42
threonyl-tRNA synthetase	TARS	-1.78	-2.27
Inflammatory and immune related group			
major histocompatibility complex, class I, A	HLA-A	2.90	1.31
MHC class II DQ-beta associated with DR2, DQw1 protein	HLA-DQB1	2.78	2.23
major histocompatibility complex, class II, DQ beta 1	HLA-DQB1	2.33	1.02
major histocompatibility complex, class II, DM beta 1	HLA-DMB	2.28	2.42
lymphocyte antigen 64 (mouse) homolog, radioprotective, 105 kD	LY64	2.23	0.89
platelet-activating factor receptor	PTAFR	-2.86	-1.94
major histocompatibility complex, class II, DN alpha	HLA-DNA	-2.50	-1.74
interleukin 9	IL9	-2.37	-1.81
chemokine (C-C motif) receptor 6	CCR6	-2.36	-2.75
small inducible cytokine A5	SCYA5	-2.30	-1.62
GRO2 oncogene	GRO2	0.74	3.41
interferon induced transmembrane protein 2	1-8D	-1.93	-3.05
major histocompatibility complex, class I, C	HLA-C	-1.81	-2.66
interleukin 10 receptor, beta	IL10RB	-1.75	-2.64
small inducible cytokine subfamily A (Cys-Cys), member 16	SCYA16	-1.90	-2.15
small inducible cytokine subfamily A (Cys-Cys), member 14	SCYA14	0.61	-2.03
Transport related group			
ubiquinol-cytochrome c reductase, Rieske iron-sulfur polypeptide-like 1	UQCRFSL1	2.83	2.20
nucleoporin 214 kD (CAIN)	NUP214	2.13	1.07
vimentin	VIM	-3.08	-3.61
ferritin, heavy polypeptide 1	FTH1	-2.15	-2.23
P glycoprotein 1/multiple drug resistance 1	PGY1	0.41	2.86
Metabolism related group			
proteasome (prosome, macropain) subunit, alpha type, 1	PSMA1	4.70	4.32
8-oxoguanine DNA glycosylase	OGG1	2.10	2.12
acetyl-coenzyme A acetyltransferase 2	ACAT2	2.08	0.40
ubiquitin-conjugating enzyme E2I (homologous to yeast UBC9)	UBE2I	0.93	2.17
damage-specific DNA binding protein 1 (127 kD)	DDB1	-1.60	-2.89
Cell proliferation and cell cycle related group			
singed (Drosophila)-like (sea urchin fascin homolog like)	SNL	2.87	3.52
cyclin B1	CCNB1	-3.22	-1.70
hepatocyte growth factor (hepapoietin A; scatter factor)	HGF	-2.53	-2.30
midkine (neurite growth-promoting factor 2)	MDK	-2.40	-1.84
Wee1 + (S. pombe) homolog	WEE1	-2.15	-2.72
polo (Drosophila)-like kinase	PLK	-2.07	-2.47
Cell differentiation and bone development related group			
similar to latent transforming growth factor beta binding protein 1	TGFBBP1	2.75	-0.31
bone morphogenetic protein 2	BMP2	2.56	1.63
GDF-1 embryonic growth factor	GDF1	2.37	1.17
catenin (cadherin-associated protein), beta 1 (88 kD)	CTNNB1	2.16	1.85
fibroblast growth factor 12	FGF12	-4.70	-4.30
fibroblast growth factor receptor 3	FGFR3	-2.28	0.18

Normal bone function is assured when there is equilibrium between bone formation and bone resorption. Apoptosis, or programmed cell death, is characterized by the activation of cysteine proteases called caspases, which cleave proteins essential for the survival of the cell. A member of this family, caspase-1, has been identified by its ability to proteolytically cleave and activate the inactive precursor of interleukin-1, a cytokine involved in the processes such as inflammation, septic shock, and wound healing. This gene has been shown to induce cell apoptosis and may function in various developmental stages¹⁰. We found that Zr and Nb Ti induced apoptosis in osteoblasts in our in vitro model system, and caspase-1 was involved in this process. The increased susceptibility to apoptosis of the less mature osteoblast could have important consequences for bone remodeling.

In our experiment, we observed several genes related with signal transduction for bone formation. However the expression of these genes such as MAP4K2, G protein coupled receptor 37, and G protein coupled receptor 9 were different according to different ceramic-coatings on Ti surfaces. MAP4K2 is a member of the kinase family. MAP kinases act as an integration point for multiple biochemical signals and are involved in a wide variety of cellular processes such as proliferation, differentiation, transcription regulation and development. MAP3K8 was identified by its oncogenic transforming activity in cells. The encoded protein is a member of the serine/threonine protein kinase family. This kinase can activate both the MAP kinase and JNK kinase pathways. This kinase was shown to activate I κ B kinases, and thus induce the nuclear production of NF- κ B. This kinase was also found to promote the production of TNF- α and IL-2 during T lymphocyte activation. Studies of a similar gene in rat suggested the direct involvement of this kinase in the proteolysis of NF- κ B1, p105 (NFKB1). This gene may also utilize a downstream in-frame translation start codon, and thus produce an isoform containing a shorter N-terminus. The shorter isoform has been shown to display weaker transforming activity^{12,15,20}. In our experiment, we noted the down-regulation of MAP4K2 on Zr surfaces. CD183 is a G protein-coupled receptor with selectivity for three chemokines, termed IP10, Mig and I-TAC. IP10, Mig and I-TAC belong to the structural subfamily of CXC chemokines, in which a single amino acid residue separates the first two of four highly conserved Cys residues. Historically, CD183 is the third CXC chemokine receptor discovered and, therefore, commonly designated as CXCR3. Binding of chemokines to CD183 induces cellular responses that are involved in

leukocyte traffic, most notably integrin activation, cytoskeletal changes and chemotactic migration. Inhibition by Bordetella pertussis toxin suggests that heterotrimeric G protein of the Gi-subclass couple to CD183. Signal transduction has not been further analyzed but may include the same enzymes that were identified in the signaling cascade induced by other chemokine receptors. As a consequence of chemokine-induced cellular desensitization (phosphorylation-dependent receptor internalization), cellular responses are typically rapid and short in duration. Cellular responsiveness is restored after dephosphorylation of intracellular receptors and subsequent recycling to the cell surface. A hallmark of CD183 is its prominent expression in in vitro cultured effector/memory T cells, and in T cells present in many types of inflamed tissues. In addition, IP10, Mig and I-TAC are commonly produced by local cells in inflammatory lesion, suggesting that CD183 and its chemokines participate in the recruitment of inflammatory cells¹⁵. In our experiment, we noted the down-regulation of G protein coupled receptor 37 on Zr surfaces, and an down-regulation of G protein coupled receptor 9 on Zr surfaces.

We demonstrated that different ceramic-coatings on Ti surfaces were capable of modulating the expressions of some genes. Our results indicated that the gene encoding bone formation-related proteins was up-regulated mainly in the Zr and Nb cultures. Carinci *et al.*¹⁸ reported that surface topography exerted influences on the frequency and amount of formed bone, and that mineralized products can be guided by the surface topography of the implant. It has also been determined that bone formation induced by osteoblast-like cells at the implant-cell interface is quite a complex process, and involves a host of cellular functions, including cellular attachment, migration, and proliferation, followed by the expression of markers for osteoblast phenotype, and the synthesis, deposition, and mineralization of the bone matrix²¹. We believe that the data reported that the function of the signaling pathway in osteoblast differentiation may contribute to the identification of new therapeutics, for the treatment of poor bone quality. This study may provide dentists with a great deal of useful information for the improvement of present biomaterials, as well as the future development of new biomaterials.

Methods

Titanium Preparation

All Ti substrates were constructed from grade 5 (Ti-

6Al-4V) titaniums. The materials were Ti discs with a diameter of 10 mm, a thickness of 1 mm, in a coin-shaped circle. The Ti samples used in the experiments had different surfaces (control; non ceramic-coating on Ti surface, Zr; zirconium-coating on Ti surface, Nb; Niobium-coating on Ti surface). Zirconium was coated on titanium surface by using plasma spraying, and Niobium was coated on titanium surface by using Physical Vapour Deposited (PVD) type coatings by O.M.T. (Luebeck, Germany). Table 1 shows these surface properties. After surface preparation, these samples were washed with distilled water, and then rinsed thoroughly in 70% ethanol and absolute ethanol. Prior to cell culturing, the discs were sterilized by γ -rays.

Cell Culture

MG63 cells were cultured on dental materials with different surfaces (control, Zr, and Nb). The MG63 cells (KCLB[®] Korean Cell Line Bank) were cultured in (Dulbecco Eagle's minimum essential medium, Biowhittaker, Belgium) MEM medium with 10% fetal bovine serum, and antibiotics (Penicillin 100 U/mL and Streptomycin 100 μ g/mL, Invitrogen, Milano, Italy) were seeded at 1×10^4 /mL in a humidified atmosphere of 5% CO₂ at 37°C. These materials were placed in a 24-multiwell plate (NUNC[™], Denmark). 1 mL of cell suspension was applied carefully to a 24-multiwell and the cells had been allowed to attach for 3 days to the MG63.

Scanning Electron Microscopy (SEM)

SEM (S-4700, HITACHI, Tokyo, Japan) was employed in order to determine the morphological characteristics of cells in culture. The advantages associated with SEM include its large depth of focus, high lateral resolution down to the nanometer range, the feasibility to study structures with high aspect ratios, and the direct production of surface images.

Human cDNA Microarray

A MG63 cDNA microarray was derived principally from a commercially available master set of approximately 15,000 human verified-sequences (Research Genetics, Inc., Huntsville, AL). The 15,000 human cDNA clone set was sorted for a list of genes (1,152 elements) representing families such as differentiation, development, proliferation, transformation, cell cycle progression, immune response, transcription and translation factors, oncogenes, and molecules involved in cell growth and maintenance. PCR-amplified cDNAs were spotted on nylon membranes. The general methodology of arraying is based on the procedures of DeRisi *et al*²².

RNA Preparation and cDNA Radiolabeling

The RNA was isolated from cultured cells which adhered to the retrieved implants of different surfaces (control, Zr, and Nb) with Trizol (Invitrogen, Milano, Italy). RNA was quantified via UV spectrophotometry (spectrophotometer-DU650; Beckman, Somerset, NJ, USA). After quantification, 3-10 μ g of total RNAs prepared from the MG63-treated dental materials with different surfaces (control, Zr, and Nb) were used for each sample for adjustment of different cell numbers. To synthesize ³³P-labeled cDNAs, quantified RNA were labeled in a reverse transcription reaction containing 5X first strand PCR buffer, 1 μ g of 24-mer poly dT primer, 4 μ L of 20 mM each dNTP excluding dCTP, 4 μ L of 0.1 M DTT, 40 U of RNase inhibitor, 6 μ L of 3,000 Ci/mmol α -³³P dCTP to a final volume of 40 μ L. The mixture was heated at 65°C for 5 min, followed by incubation at 42°C for 3 min. Two μ L (specific activity: 200,000 U/mL) of Superscript II reverse transcriptase (Invitrogen, Milano, Italy) was then added and the samples were incubated for 30 min at 42°C, followed by the addition of 2 μ L of Superscript II reverse transcriptase and another 30 min of incubation. Five μ L of 0.5 M EDTA was added to chelate divalent cations. After the addition of 10 μ L of 0.1 M NaOH, the samples were incubated at 65°C for 30 min to hydrolyze remaining RNA. Following the addition of 25 μ L of 1 M Tris (pH 8.0), the samples were purified using Bio-Rad 6 purification columns (Hercules, CA, USA). This resulted in 5×10^6 to 3×10^7 cpm per reaction²³.

Hybridization and Scanning

cDNA microarrays were pre-hybridized in hybridization buffer containing 4.0 mL Microhyb (Invitrogen, Milano, Italy), 10 μ L of 10 mg/mL human Cot 1 DNA (Invitrogen, Milano, Italy), and 10 μ L of 8 mg/mL poly dA (Pharmacia, Peapack, NJ). Both Cot 1 and poly dA were denatured at 95°C for 5 min prior to use. After 4 h of pre-hybridization at 42°C, approximately 10^7 cpm/mL of heat-denatured (95°C, 5 min) probes were added and incubation continued for 17 h at 42°C. Hybridized arrays were washed three times in 2X SSC and 0.1% SDS for 15 min at room temperature. The microarrays were exposed to phosphorimager screens for 1-5 days, and the screens were then scanned in a FLA-8000 (Fuji Photo Film Co., Japan) at 50 μ m resolution^{23,24}.

Data Analysis

Microarray images were trimmed and rotated for further analysis using L-Processor system (Fuji Photo Film Co., Japan). Gene expression of each microarray was captured by the intensity of each spot pro-

duced by radioactive isotopes. Pixels per spot were counted by Arraygauge (Fuji Photo Film Co., Japan) and exported to Microsoft Excel (Microsoft, Seattle, WA, USA). The data were normalized with Z transformation to obtain Z scores by subtracting each average of gene intensity and dividing with each standard deviation. Z scores provide each of 2,304 spots (two sets of 1,152 genes) genes with the distance from the average intensity and were expressed in units of standard deviation. Thus, each Z score provides flexibility to compare different sets of microarray experiments, by adjusting differences in hybridization intensities. Gene expression difference as compared with untreated control cells were calculated by comprising Z score differences (Z differences) among the same genes. This facilitates comparing each gene that had been up- or downregulated as compared with the control cells. Z differences were calculated first by subtracting Z scores of the controls from each Z score of the sample. These differences were normalized again to distribute their position by subtracting the average Z difference and dividing with the standard deviation of the Z differences. These distributions represent the Z ratio value and provide the efficiency for comparing each microarray experiment²³. Scatter plots of intensity values were produced by Spotfire (Spotfire, Inc., Cambridge, MA)²⁵. Cluster analysis was performed on the Z-transformed microarray data by using two programs available as shareware from Michael Eisen's laboratory (<http://rana.lbl.gov>). Clustering of changes in gene expression was determined by using a public domain cluster based on pair wise complete-linkage cluster analysis²⁶.

Acknowledgements

We thank Dr. Yoon S. Cho-Chung (Cellular Biochemistry Section, Basic Research Laboratory, CCR, NCI, NIH, Bethesda, MD) and Dr. Kevin G. Becker (DNA Array Unit, NIA, NIH, Baltimore, MD) for valuable advices on cDNA microarray. This study was supported by a grant of Medical Research Center for Environmental Toxicogenomic and Proteomics, funded by Korea Science and Engineering Foundations and Ministry of Science & Technology, a grant of the Korea Health 21 R&D Project, Ministry of Health & Welfare, Republic of Korea (Hmp-00-GN-01-0002 & KPGRN-R-04), a Korea Institute of Science & Technology Evaluation and Planning (KISTEP) and Ministry of Science & Technology (MOST), Korean government, through its National Nuclear Technology Program, and a grant No. R01-2001-000-00212-0 from the Basic Research Program

of the Korea Science & Engineering Foundation.

References

1. Shah, A.K. *et al.* High-resolution morphometric analysis of human osteoblastic cell adhesion on clinically relevant orthopedic alloys. *Bone* **24**(5) 499-506 (1999).
2. Cooper, L.F. *et al.* Incipient analysis of mesenchymal stem-cell-derived osteogenesis. *J Dent Res.* **80**(1), 314-320 (2001).
3. Carinci, F. *et al.* Titanium-cell interaction: analysis of gene expression profiling. *J Biomed Mater Res.* **66 B**(1), 341-346 (2003).
4. Viornery, C. *et al.* Osteoblast culture on polished titanium disks modified with phosphonic acids. *J Biomed Mater Res.* **62**(1), 149-155 (2002).
5. Kim, H.K., Jang, J.W. & Lee, C.H. Surface modification of implant materials and its effect on attachment and proliferation of bone cells. *J Mater Sci Mater Med.* **15**(7), 825-830 (2004).
6. Ogawa, T., Sukotjo, C. & Nishimura, I. Modulated bone matrix-related gene expression is associated with differences in interfacial strength of different implant surface roughness. *J Prosthodont* **11**(4), 241-247 (2002).
7. Schneider, G.B. *et al.* Implant surface roughness affects osteoblast gene expression. *J Dent Res.* **82**(5), 372-376 (2003).
8. Carinci, F. *et al.* Zirconium oxide: analysis of MG63 osteoblast-like cell response by means of a microarray technology. *Biomaterials* **25**(2), 215-228 (2004).
9. Orsini, G. *et al.* Surface analysis of machined versus sandblasted and acid-etched titanium implants. *Int J Oral Maxillofac Implants* **15**(6), 779-784 (2000).
10. Son, W.W. *et al.* In vivo histological response to anodized and anodized/hydrothermally treated titanium implants. *J Biomed Mater Res B Appl Biomater.* **66**(2), 520-525 (2003).
11. Ogawa, T. & Nishimura, I. Different bone integration profiles of turned and acid-etched implants associated with modulated expression of extracellular matrix genes. *Int J Oral Maxillofac Implant* **18**(2), 200-210 (2003).
12. Kim, C.S. *et al.* Effect of various implant coatings on biological responses in MG63 using cDNA microarray. *J Oral Rehabil.* **33**, 368-379 (2006)
13. Kim, C.S. *et al.* Gene-expression profiling of titanium-cell interaction. *J Korea Acad Prosthodont.* **43**(3), 393-408 (2005).
14. Sohn, S.H. *et al.* Biological effects of different thin layer hydroxyapatite coatings on anodized titanium. *Mol. Cell. Toxicol.* **1**(4), 237-247 (2005).
15. Carinci, F. *et al.* Analysis of osteoblast-like MG63 cells' response to a rough implant surface by means of DNA microarray. *J Oral Implantol.* **29**(5), 215-220

- (2003).
16. Hornez, J.C. *et al.* Multiple parameter cytotoxicity index on dental alloys and pure metals. *Biomol Eng.* **19**(2-6), 103-117 (2002).
 17. Monsees, T.K. *et al.* Effects of different titanium alloys and nanosize surface patterning on adhesion, differentiation, and orientation of osteoblast-like cells. *Cells Tissues Organs* **180**(2), 81-95 (2005).
 18. Carinci, F. *et al.* Analysis of MG63 osteoblastic-cell response to a new nanoporous implant surface by means of a microarray technology. *Clin Oral Implants Res.* **15**(2), 180-186 (2004).
 19. Lossdorfer, S. *et al.* Microrough implant surface topographies increase osteogenesis by reducing osteoclast formation and activity. *J Biomed Mater Res.* **70A**(3), 361-369 (2004).
 20. Chaudhary, L.R., Hofmeister, A.M. & Hruska, K.A. Differential growth factor control of bone formation through osteoprogenitor differentiation. *Bone* **34**(3), 402-411 (2004).
 21. Mustafa, K. *et al.* Determining optimal surface roughness of TiO₂ blasted titanium implant material for attachment, proliferation and differentiation of cells derived from human mandibular alveolar bone. *Clin Oral Implants Res.* **12**(5), 515-525 (2001).
 22. DeRisi, J. *et al.* Use of a cDNA microarray to analyse gene expression patterns in human cancer. *Nat Genet.* **14**(4), 457-460 (1996).
 23. Vawter, M.P. *et al.* Application of cDNA microarrays to examine gene expression differences in schizophrenia. *Brain Res Bull.* **55**(5), 641-650 (2001).
 24. Park, G.H. *et al.* Genome-wide expression profiling of 8-chloroadenosine- and 8-chloro-cAMP-treated human neuroblastoma cells using radioactive human cDNA microarray. *Exp Mol Med.* **34**(3), 184-193 (2002).
 25. Tanaka, T.S. *et al.* Genome-wide expression profiling of mid-gestation placenta and embryo using a 15,000 mouse developmental cDNA microarray. *Proc Natl Acad Sci USA.* **97**(16), 9127-9132 (2000).
 26. Eisen, M.B. *et al.* Cluster analysis and display of genome-wide expression patterns. *Proc Natl Acad Sci USA.* **95**(25), 14863-14868 (1998).